Mon. Not. R. astr. Soc. (1971) **154**, 229–253.

ATMOSPHERIC LIMITATIONS TO THE ANGULAR RESOLUTION OF APERTURE SYNTHESIS RADIO TELESCOPES

Richard Hinder and Martin Ryle

(Received 1971 May 19)

SUMMARY

The technique of aperture synthesis has reached a stage where it is technologically feasible to construct a radio telescope several tens of kilometres in extent. The angular resolution of maps made with such an instrument on the surface of the Earth would, however, be limited by refraction in the troposphere and the ionosphere. Tropospheric irregularities having a scale size of about 1 km set a limit to the operation of large synthesis telescopes at the higher frequencies whilst ionospheric irregularities having a scale size of about 100 km become a hindrance at the lower frequencies. The permissible observing wavelengths and baselines are further limited by a systematic refraction due to the curvature of the Earth. A numerical simulation of the effects of the irregularities on the synthesized response of a typical instrument, and a consideration of the effects of systematic refraction, show that the limiting resolution of a telescope in middle latitudes is in the range 0·1–1″ arc. In principle the effects of refraction could be reduced by determining the atmospheric parameters along the ray paths throughout the period of observation and applying suitable corrections. The effects of systematic refraction could be greatly reduced by this procedure, but it would in practice be extremely difficult to achieve an accuracy sufficient to correct for the effects of irregularities.

1. INTRODUCTION

Throughout the history of their subject radio astronomers have been continually restricted by the comparatively low angular resolution of the instruments at their disposal. Although the technique of long baseline interferometry with independent local oscillators has recently proved valuable in studying very compact regions, the absence of phase information and the incomplete coverage of the aperture plane are severe limitations; the development of credible physical models of radio sources is unlikely until full maps of the objects are available with greater angular resolution than has so far been achieved.

The engineering problems associated with the construction of precise paraboloids have so far limited their attainable angular resolution to a few minutes of arc. A resolution of $\approx 1'$ arc has been obtained for instruments having a diameter of up to ≈ 5 m, but the available signal-to-noise ratio is then too small for many of the observations desired. Although designs using active surface correction to achieve a higher accuracy have been considered, the cost of such instruments with resolutions significantly better than $1'$ arc is likely to be prohibitive.

The technique of aperture synthesis (Ryle & Hewish 1960) can, however, provide very much greater resolution and sensitivity than the largest paraboloids envisaged. The Cambridge One-Mile telescope (Elsmore, Kenderdine & Ryle 1966), for example, has an angular resolution of 6″ arc at a wavelength of 6 cm,

and an effective collecting area corresponding to that of a dish ≈ 400 m in diameter. Other, even more powerful, telescopes making use of this principle are now available or under construction.

Whilst circumventing the engineering problems associated with large structures, stable against gravity and wind loads, aperture synthesis requires two or more smaller dishes mounted on stable foundations, the relative positions of which are known with a precision appropriate to the wavelength of operation, together with radio frequency connections between the aerials and the receiver having a differential path which is correspondingly stable. Conventional surveying techniques are barely adequate to fix the relative positions of aerial elements with sufficient precision, but fortunately this can be done from the radio observations themselves if a few sources having small angular diameters and known positions are available. A number of such calibration sources are believed to coincide with compact optical objects whose positions have been measured with an accuracy of 0·1″ arc (Murray, Tucker & Clements 1969). The application of this method to establish the geometry of the One-Mile telescope with a precision of ~ 1 mm is described elsewhere (Elsmore and Smith, in preparation). Even if the positions of the calibration sources were not known accurately it would still be possible to obtain internally consistent source maps, although there would then be uncertainties in their coordinates corresponding to those of the calibration sources.

If the problems of providing phase-stable electronics and connections between the elements of such an instrument can be overcome, as now seems probable, the successful operation depends on the phase irregularities produced in an incident wavefront by variations of the refractive index of the atmosphere. It is evident that unless these are much less than one radian across the whole aperture of the instrument they may be the principal limiting factor and the intended angular resolution will not be achieved. Variations of refractive index in the atmosphere may be introduced either by fluctuations of the water vapour content in the troposphere or by variations of the electron content in the ionosphere. The former produce a path difference between two points in the wavefront which is independent of wavelength λ; the ionospheric variations, on the other hand, produce differential path variations which increase as λ^2.

The presence of phase irregularities across the aperture introduces sidelobe responses and reduces the forward gain. The maximum tolerable level of sidelobe responses depends on the type of radio source being investigated. For example, in observations of complex sources whose active regions subtend ~ 100 beam areas, serious errors in the apparent distribution of surface brightness may be caused by sidelobes having a r.m.s. level of 1 per cent relative to the main response; in observations of more compact sources subtending less than 10 beam areas a sidelobe level of up to 3 per cent r.m.s. may be permissible.

The aim of the present paper is to assemble the data available on the phase variations imposed on a wave traversing the atmosphere, and to assess the effect they will have on limiting the performance of very large radio telescopes of the synthesis type. Variations of refractive index also occur outside the Earth's atmosphere—both in the interplanetary and interstellar media—but these produce effects very much smaller than those caused by the ionosphere. They may, however, impose a limitation on radio astronomical observations from outside the atmosphere.

This analysis formed part of the design study for a new telescope similar in

principle to the One-Mile telescope. This is the 5-km radio telescope, now under construction (*Nature*, **221**, 515, 1969). The detailed analysis of the effects of wavefront irregularities on the reception pattern has therefore been based on the geometry of this particular type of instrument in order to assess the overall dimensions and operating wavelength which will provide the maximum resolving power, and to determine how the operation at any given wavelength will be affected at different times of day, season, and solar epoch.

An elementary analysis of the performance of synthesis instruments in the presence of irregularities in the wavefront is presented in Section 2. The maximum level of sidelobe responses tolerable in various kinds of observation is derived in Section 3. The differential path variations imposed by the troposphere and ionosphere are discussed in Sections 4 and 5 respectively. The results are then used to compute the effect on an instrument having the general design features of the 5-km radio telescope but of arbitrary size and operating wavelength, so that it is possible to determine the deterioration in performance, as a function of season and solar epoch, of a range of different instruments. In this way the maximum resolving power which it is possible to obtain at the surface of the earth in temperate latitudes is found. There are not sufficient data available to assess how this value will change at other geographical locations, but methods are suggested for evaluating the suitability of any observing site.

2. THE EFFECT OF PHASE ERRORS ACROSS THE APERTURE

In its most elementary form the technique of aperture synthesis employs two small aerial elements of diameter d which are used together with a correlation receiver to measure, in turn, the components of the two-dimensional Fourier transform of the distribution of sky brightness within the whole field of view of the elements. If the desired resolution is that of an aperture of diameter D, it is necessary to arrange the elements in each of $\sim D^2/d^2$ configurations, the maximum separation being D (Fig. 1(a)). The results of these observations are then combined by Fourier transformation to provide a map of sky brightness.

If the required map extends over a solid angle smaller than that of the reception pattern of the individual elements, as in the case of observations to determine the structure of individual sources considerably more intense than others in the reception pattern, a smaller number of configurations may be sufficient, in the form of a grating (Elsmore *et al.* 1966). The separation of successive sampling points must then not exceed $\approx \lambda/\theta$ where θ is the angular diameter of the source and the total number of samples is $\sim D^2\theta^2/\lambda^2$.

A particularly simple structural arrangement is that of the One-Mile telescope, in which the elements are placed successively at different spacings on an east–west line, and at each spacing track an area of sky for 12 hr, so that the relative positions of the elements correspond to the movement of one in a semi-circular path about the other (Fig. 1(b)). In this case each of the sampling points necessary to define one term in the Fourier transform is based on an observing time of $\approx 230\ d/D$ minutes at the largest separation D, and a longer time, inversely proportional to the separation, for smaller separations. For grating observations the integration time for each sample is increased by the ratio of the incremental separation to d.

Suppose now that each sample is recorded with a phase error having an r.m.s. value $\Delta\phi$, much less than 1 radian, and that the errors in successive samples are

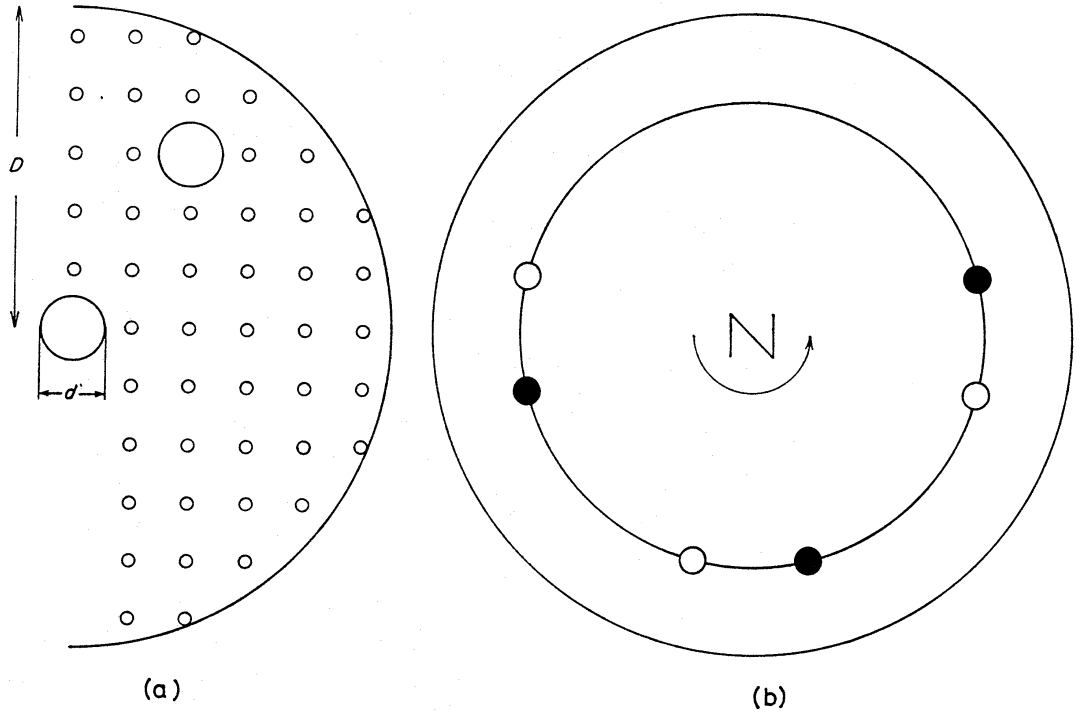

FIG. 1.(a) *The synthesis of a circular aperture of diameter D by measuring the correlation between the signals received by a central aerial and movable aerial which occupies successively each of the points shown in the half circle.*
(b) *The principle of earth-rotation synthesis. Looking down on the Earth from the north celestial pole the black aerial moves around the white aerial, sweeping out a half circle in 12 hr.*

uncorrelated. After the Fourier transformation the errors appear as a reduction of the main response and as sidelobe responses distributed uniformly over the map. The magnitude of the sidelobe responses relative to the main response is of the order $\Delta\phi n^{-1/2}$ r.m.s. where n is the total number of samples in the aperture. For a complete mapping of the whole field of view of the aerials according to the simple scheme of Fig. 1(a), $n \sim D^2/d^2$ and the r.m.s. sidelobe level is $\approx \Delta\phi(d/D)$.

In practice the phase errors imposed by atmospheric irregularities depend on the separation of the aerials, tending to zero at small separations. In addition samples observed at the larger separations are normally given less weight than those observed at the smaller separations so that the resulting response has a lower level of sidelobes than the unweighted response, whilst retaining almost the same resolving power. Furthermore, the irregularities may have a correlation time much less than the sampling period so that the final error is smaller than the fluctuations present in the wavefront. On the other hand some irregularities may have a time scale longer than the sampling period, in which case the error introduced in successive samples may not be independent; under these circumstances the sidelobes are likely to be larger than $\Delta\phi n^{-1/2}$.

In systems having more than one pair of aerials, observations at more than one spacing are obtained simultaneously. Depending on the physical scale of the irregularities in the incident wavefront, there may then be some correlation between the errors appearing in samples from different pairs of aerials. Under these conditions there will be an enhancement of the sidelobes in certain regions of the map.

In order to determine the effect of atmospheric irregularities on the performance of a particular instrument it is therefore necessary to know firstly the variation of the instantaneous phase error between two lines of sight as a function of their separation, and secondly the time scale of the phase error, and whether this is caused by the formation and decay of irregularities or by the horizontal drift of an effectively unchanging pattern of irregularities across the telescope.

Owing to the statistical nature and complexity of the problem the sidelobe levels occurring under various conditions have been determined from the known characteristics of the atmosphere, presented in Sections 4 and 5, by a numerical simulation technique, the results of which are described in Section 6. Firstly, however, the maximum level of sidelobe responses acceptable in various kinds of observation is examined.

3. THE MAXIMUM ACCEPTABLE LEVEL OF SIDELOBE RESPONSES

In an evaluation of the performance of a telescope it is important to establish the maximum level of sidelobes which is tolerable on the maps produced by the instrument. The maximum acceptable level depends on the detail with which the sources can be analysed, and thus depends both on the degree to which the source is resolved, and on the signal to noise ratio. The criterion adopted in the present analysis is that the r.m.s. error in surface brightness on the map due to sidelobes should be no more than 10 per cent of the mean brightness temperature averaged over the active regions of the source.

The errors of brightness temperature on the map are, of course, related to the r.m.s. level of sidelobes α in the response pattern of the synthesis. It is, however, also dependent on the source structure and on the distribution of the sidelobes within the response pattern. The limiting value of α which produces the maximum tolerable level of sidelobes on the map clearly varies over a wide range; in particular it depends on how well the components of the source are resolved.

As an illustration let us examine the limiting value of α which is tolerable in an observation of a source which occupies N beam areas and whose effective brightness temperatures vary over a range comparable with the mean brightness temperature of the source. It is initially assumed that the sidelobe responses are distributed uniformly over the entire response pattern. In this case the r.m.s. error on the map is $\approx N^{1/2}\alpha$, since the sidelobes from each of the N components add incoherently, and the limiting value of α is accordingly $0{\cdot}1\ N^{-1/2}$. Clearly, if N is very large α must be correspondingly very small.

For N less than about 10 the source is barely resolved, and the chief interest may lie in a derivation of the angular width or in the existence of weak subsidiary components. In such cases a sidelobe level of up to 5 per cent of the main response can be tolerated. In the case of more extensive sources N may be in the range 10^2–10^4 and the limiting level of sidelobes may have to be restricted to a value as small as 0·3 per cent of the main response. However, the increased number of sampling points n required to map the more extensive sources reduces the sidelobe level and compensates for the smaller level of sidelobes required. Generally, a tolerable sidelobe level can be attained in the presence of random phase errors which are up to 0·1 radians r.m.s. at each sampling point.

Whilst irregular atmospheric refraction leads to the uniform distribution of sidelobes considered above, systematic atmospheric refraction produces sidelobes

which are restricted to a region very close to the main response. In such cases a sidelobe level of 10 per cent relative to the main response will be taken as the limiting value.

4. PHASE VARIATIONS IMPOSED BY THE TROPOSPHERE

Refraction in the troposphere produces an increase in the phase path length of a radio wave passing through it by an amount ΔL in excess of the geometrical path length; this increase is independent of wavelength. The refractive index depends on the total air pressure, the temperature and the water vapour pressure, and is usually defined in terms of the radio refractivity, which is the departure of the refractive index from unity, measured in parts per million. The refractivity of the air is about 300 at ground level, and falls exponentially with increasing height, becoming $1/e$ of the surface value at a height of about 7 km.

The operation of a synthesis radio telescope is affected by differences in the phase paths from a source to the separate elements. The difference between the phase paths to a pair of elements will be called the *differential path*. Refraction in the troposphere produces three distinct kinds of differential path which are described below.

4.1 *Irregularities having a scale size of* ≈ 700 *m*

Irregular refraction has been studied using interferometric observations of radio sources at 11 cm wavelength by Baars (1967) and by Basart, Miley & Clark (1970) at the U.S. National Radio Astronomy Observatory; at 11-cm wavelength by Gent, Adgie & Crowther (1969) at the Royal Radar Establishment, Malvern; and at both 11-cm and 6-cm wavelength by Hinder (1970) using the One-Mile telescope at Cambridge.

Hinder (in preparation) has carried out a detailed investigation of the nature of the irregularities occurring over Cambridge which shows that the magnitude of the effect is strongly dependent on the time of day and the season; at elevations greater than $\approx 30°$ the r.m.s. variation of ΔL is $\approx 2{\cdot}3$ mm in the summer day-time, but varies from day to day between 1 mm and 6 mm. During the summer night-time and throughout the winter the variations are less by a factor of up to 10. The irregularities move with the wind at a height of 1 to 2 km and have a scale size between 300 and 1200 m, with an average value of 700 m. The One-Mile telescope is capable of detecting scales up to ~ 10 km provided that the extra path with which they are associated is comparable with that found for the smaller scale sizes, but no scales greater than ≈ 1200 m have been detected. Observations by Basart *et al.* (1970) using a baseline of 11 km have given some evidence for the occasional existence of scale sizes greater than 1 km, but it is possible that these might be associated with the incidence of large scale weather systems discussed below. The irregularities observed so far are attributed to fluctuations of water vapour pressure associated with convection, and can occur in conjunction with cumulus clouds, and in clear air.

4.2 *Large scale weather systems*

In addition to irregular structure on a scale of ≈ 700 m, gradients of pressure, temperature and water vapour pressure associated with frontal systems may be important. From data presented by Bean & Dutton (1966), it appears that typical

warm and cold fronts produce a differential path between two lines of sight, at an elevation of 30° on a baseline normal to the front, of ≈20 mm per 100 km of baseline. With ground-based measurements of pressure, temperature and humidity, it should be possible to correct the differential paths introduced by most weather systems to an accuracy of 20 per cent, corresponding to uncertainties of ≈4 mm per 100 km of baseline. A few situations will doubtless introduce uncertainties in excess of this value, but are likely to occur for such a small proportion of the time as to be irrelevant in the present context.

4.3 *Curvature of the troposphere*

A spherically stratified atmosphere introduces a differential path between a source and two separated aerial elements owing to the different elevation angles of the source at the two aerials. The magnitude of the effect increases rapidly with zenith angle and is approximately proportional to the separation of the aerial elements, as shown in Table I, where the effect has been evaluated for a source observed at an azimuth along the baseline. The effect is absent for a source normal to the baseline.

TABLE I

The differential path in mm due to the curvature of the atmosphere for a source at an azimuth along the baseline.

Baseline	Elevation			
(km)	5°	10°	20°	45°
1	38	11	3	1
10	380	110	28	5
100	3800	1100	280	50

The values have been calculated by approximating the troposphere by a layer having a constant refractive index and a thickness equal to the scale height. This approximation is valid if the increase of path length due to bending of the ray path within the troposphere is negligible in comparison with that due to the reduction of the phase velocity, which is true for all elevations greater than about 3° (Bean & Dutton 1966). In practice the effect will differ slightly from the tabulated values owing to deviations of the altitude profile of refractive index from its mean exponential form, but surface measurements of pressure, temperature and humidity will probably be sufficient to enable the differential path to be estimated to within 10 per cent of the true value.

4.4 *The total effect of tropospheric refraction*

The total effect of refraction in the troposphere is shown in Table II where, for an elevation angle of 30° and an azimuth along the baseline, the uncertainty in the path difference to two aerial elements separated by 1, 10 and 100 km is given for each of the above effects. It is assumed that corrections deduced from surface measurements of pressure, temperature and humidity have been included (the uncorrected values of differential path are shown in parentheses).

It is evident that, for telescopes of total aperture less than 10 km, the limitations imposed by the troposphere are due almost entirely to the small scale irregularities of water vapour pressure. For apertures much greater than 10 km the

uncertainties in the differential path imposed by the curvature of the atmosphere predominate.

TABLE II

The differential path in mm due to different kinds of tropospheric refraction for a source observed at an elevation of 30° and an azimuth along the baseline.

Baseline (km)	Irregularities		Weather systems	Curvature
	Summer	Winter		
1	2·6	0·66	0·04 (0·2)	0·12 (1·2)
10	2·8	0·71	0·4 (2·0)	1·2 (12)
100	2·8	0·71	4 (20)	12 (121)

In principle the differential path could be estimated by measuring the appropriate atmospheric parameters along the ray paths. A number of methods have been summarized by Mathur, Grossi & Pearlman (1970). Ground-based microwave radiometric measurements of molecular line radiation at 22 and 60 GHz, from water vapour and oxygen respectively, would enable the differential path to be estimated with an uncertainty of a few centimetres (Schaper, Staelin & Waters 1970). Another method involves measurements of laser radiation scattered back by the gaseous component of the atmosphere (Cooney, Orr & Tomasetti 1969; Cooney 1970). Neither method has, however, been evaluated in an operational system, and it is likely that both will be limited by the occurrence of cloud along the line of sight. An alternative method would be to observe an unresolved source or satellite of known position during the observations, either with a separate, but simpler, telescope, or with the synthesis instrument itself. It is likely that this method could correct for the effects of both weather systems and curvature, but the lines of sight to the calibration source and the area of sky under investigation would probably be too far removed to correct for the effects of the small scale irregularities. Currently available methods of correction are unlikely to reduce the uncertainties in differential path below those shown in Table II.

5. PHASE VARIATIONS IMPOSED BY THE IONOSPHERE

The phase path length along the line of sight of a radio wave passing through the ionosphere is less than the geometrical path length by an amount which varies with the number of electrons along the line of sight and with the wavelength. The path *increase* ΔL, in metres, due to the presence of the ionosphere is given by (Davies 1965).

$$\Delta L \approx -4{\cdot}5 \times 10^{-16} \lambda^2 Q$$

where λ is the wavelength in metres and Q is the total electron content along the line of sight in electrons m^{-2}.

The mean total electron content is of the order of 10^{17} electrons m^{-2}, but shows variations with the time of day, season, solar epoch and latitude. There are times when the ionosphere is disturbed, on occasions of enhanced geomagnetic activity and after the ejection of particle showers from the Sun, but such behaviour is of little importance in the present context since it occurs for only a small proportion of the time. For the present purpose, it is sufficient to note that the range of total electron content likely to be encountered at any place and time is between 10^{16} and 10^{18} electrons m^{-2}.

As in the case of tropospheric refraction, the differential paths imposed by the ionosphere are of three distinct kinds; these are now discussed separately.

5.1 *Irregularities*

Irregularities of the total electron content exist in the ionosphere on all scales between ~ 1 km and ~ 1000 km. The irregularities have been studied most fully as an irregular component of the Faraday rotation of radio waves from satellite beacons (see e.g. Garriott, da Rosa & Ross 1970). Titheridge (1968) has employed this method in New Zealand and deduced that variations in the total electron content on scales from 10 to 400 km are caused by movement in the ionosphere rather than by evolution. Irregularities having a scale size of about 100 km have no preferred orientation, show little diurnal variation and have horizontal gradients lying between 0·5 and 2×10^{15} electrons m^{-2} per 100 km horizontal distance (Roger 1964; Bhonsle 1966; Rao 1967; Titheridge 1968). The smaller irregularities having scale sizes between 1 and 10 km are responsible for the occurrence of spread-F, principally at night-time, and for the second-to-second scintillation of radio sources at lower frequencies. Their horizontal gradients are of the same order as those of the 100-km scale sizes, and their much smaller scale size accordingly implies that their perturbation of the path through the ionosphere is correspondingly less. The larger scales, of the order of 1000 km, are more familiar as the travelling ionospheric disturbances which occur after the onset of geomagnetic storms. Their occurrence is accordingly much less frequent than that of the 100-km scale sizes, and they are consequently seldom likely to affect the operation of a radio telescope.

TABLE III

Measurements of refraction imposed by ionospheric irregularities, normalized to a wavelength of 1 m

Location	Time	Mean Sunspot number	Angular variation (minutes of arc r.m.s.)	Path variation (metres r.m.s.)	Reference
Boulder	Feb. 1958–Feb. 1959	190	0·3	6	Lawrence *et al.* (1961)
	July 1960–Sept. 1961	80	0·045	0·93	Clarke (1964)
Cambridge	Summer 1961	60	<0·024	<0·49	Williams (1964)
	Summer 1963	30	<0·018	<0·37	
	Aug. 1963–Dec. 1964	30	<0·03	<0·6	Okoye & Hewish (1968)
Aberystwyth	Apr. 1968	105	0·021	0·43	Williams (private communication)
	May 1968	154	0·040	0·82	
	Oct. 1968	86	0·019	0·39	
	Satellite measurements			min 0·2 max 0·6	

The intermediate scales, of about 100-km lateral size, have also been observed in interferometric observations of point radio sources, appearing as an angular

scintillation with a time scale of about 20 min. The extra path imposed on a line of sight by an irregularity of lateral scale X is related to the observed angular variation of the wavefront $\Delta\theta$ by

$$\Delta L = X\Delta\theta/\sqrt{2},$$

as long as the baseline is much smaller than X and the autocorrelation function of the irregularities is Gaussian. Results reported by several workers are shown in Table III, together with values obtained from Faraday rotation of satellite signals.

In deriving ΔL from angular refraction a scale size of 100 km has been assumed. The result by Lawrence, Jespersen & Lamb (1961) at Boulder, Colorado, is inconsistent with the rest of the data. The other values, at widely varying solar epochs and seasons, are satisfactorily consistent and in agreement with the satellite data; it therefore appears that the range of path variation likely to be encountered on a single line of sight due to irregularities having a scale size of about 100 km is between 0·3 and 0·9 m r.m.s. at $\lambda = 1$ m. There is some indication that the mean level changes slightly with solar epoch, the larger values occurring at sunspot maximum.

5.2 *Diurnal variation of total electron content*

Differential paths between lines of sight from the separated aerial elements can also be introduced by gradients of ionization associated with the diurnal variation of the solar zenith angle. North–south gradients have no resultant effect on an east–west baseline; diurnal variations, however, produce gradients which lie mainly from east to west. The steepest gradients, about 10^{13} electrons m^{-2} s^{-1} (Garriott & Smith 1965), occur at dawn. At middle latitudes this figure corresponds to a differential path of $1{\cdot}6\,\lambda^2$ m per 100 km of aerial separation. Conventional ionosonde measurements should enable these gradients to be determined with an uncertainty of about 20 per cent, chiefly due to the unknown amount of ionization above the level of maximum ionization density.

5.3 *Curvature of the ionosphere*

The spherical stratification of the ionosphere introduces a differential path which varies with elevation as shown in Table IV, where the values have been calculated for a total electron content of 10^{17} electrons m^{-2}, distributed uniformly in a shell of thickness 200 km and mean height 300 km above the surface of the Earth. The values refer to a wavelength of 1 m and scale as λ^2 at other wavelengths. Owing to the inherent variability of the total electron content, the range of differential paths likely to be encountered at an azimuth along the baseline is from 0·1 to 10 times the values presented in Table IV.

TABLE IV

The differential path in metres due to the curvature of the ionosphere for a source at an azimuth along the baseline. The values are normalized to a wavelength of 1 m

Baseline (km)	Elevation 5°	10°	20°	45°
1	0·020	0·029	0·024	0·008
10	0·20	0·29	0·24	0·080
100	2·0	2·9	2·4	0·80

The effect is small for a source close to the horizon at an azimuth along the baseline, since in this case the lines of sight from the two aerials traverse nearly the same path through the ionosphere. The differential path firstly increases with elevation and then decreases for elevations greater than $\approx 10°$. This behaviour is in contrast with that shown by the troposphere, where the maximum effect occurs at zero elevation. In common with the troposphere, however, the effect is approximately proportional to the baseline for separations of up to ~ 1000 km, and is absent for a source normal to the baseline. Estimates of total electron content inferred from ionosonde measurements should enable the differential path imposed by curvature to be corrected with an uncertainty of about 20 per cent.

5.4 *The total effect of ionospheric refraction*

The total effect of refraction in the ionosphere is summarized in Table V where, for an elevation of 30° and an azimuth along the baseline, the ranges of the differential paths to two aerial elements separated by 1, 10 and 100 km are tabulated for each of the effects considered above. The values for gradients and curvature are shown corrected with an uncertainty of 20 per cent; the uncorrected values are shown in parentheses.

TABLE V

The differential path in metres due to different kinds of ionospheric refraction for a source observed at an elevation of 30° *and an azimuth along the baseline. The values are normalized to a wavelength of* 1 *m.*

Baseline (km)	Irregularities (min)	(max)	Gradients	Curvature
1	0·007	0·010	<0·003 (<0·016)	0·0003–0·030 (0·0016–0·16)
10	0·071	0·099	<0·030 (<0·16)	0·003–0·30 (0·016–1·6)
100	0·56	0·79	<0·30 (<1·6)	0·030–3·0 (0·16–16)

The diurnal variation manifests itself for only a few hours each day; furthermore the quoted value is an upper limit. In most observations and for baselines up to several hundred kilometres, the irregular component of the differential path will be the principal limiting factor. Since the irregularities represent variations of a few per cent about the mean total electron content, the effects which they produce can be corrected only by measurements having an accuracy of better than a few per cent. Whilst techniques capable of this accuracy are at present being developed, using a combination of phase path length and polarization rotation measurements of geostationary satellite signals (Almeida, Garriott & da Rosa 1970) it is unlikely that the signals from the satellite would pass sufficiently close to those from the radio source to permit an adequate correction to be made. The technique of monitoring the angular variation of a known point source from a given position with a simple low frequency interferometer would suffer from the same drawback. Each of these techniques could, however, be used to correct the effects imposed by gradients and curvature to a level negligible in comparison with that imposed by the irregularities; the irregularities are accordingly a limiting factor at the longer wavelengths.

For baselines greater than ~ 100 km, the uncertainties due to curvature are greater than those due to irregularities. Observations at two widely-spaced frequencies would enable corrections to be made if the source were unresolved, but

would not be applicable to observations of complex radio sources. Such a technique would accordingly be of restricted use in most synthesis observations, but might be of value in accurate VLBI observations, either to determine the positions of unresolved radio sources or for geodetic measurements (Dickinson, Grossi & Pearlman 1970).

6. THE EFFECTS OF ATMOSPHERIC REFRACTION ON AN EIGHT ELEMENT TELESCOPE OF ARBITRARY BASELINE AND OPERATING WAVELENGTH

In this section the effects of atmospheric refraction on the operation of a synthesis telescope using the rotation of the Earth, similar in general design to the One-Mile telescope, are determined for a range of operating wavelengths λ and maximum baselines D. The configuration of the instrument is shown in Fig. 2

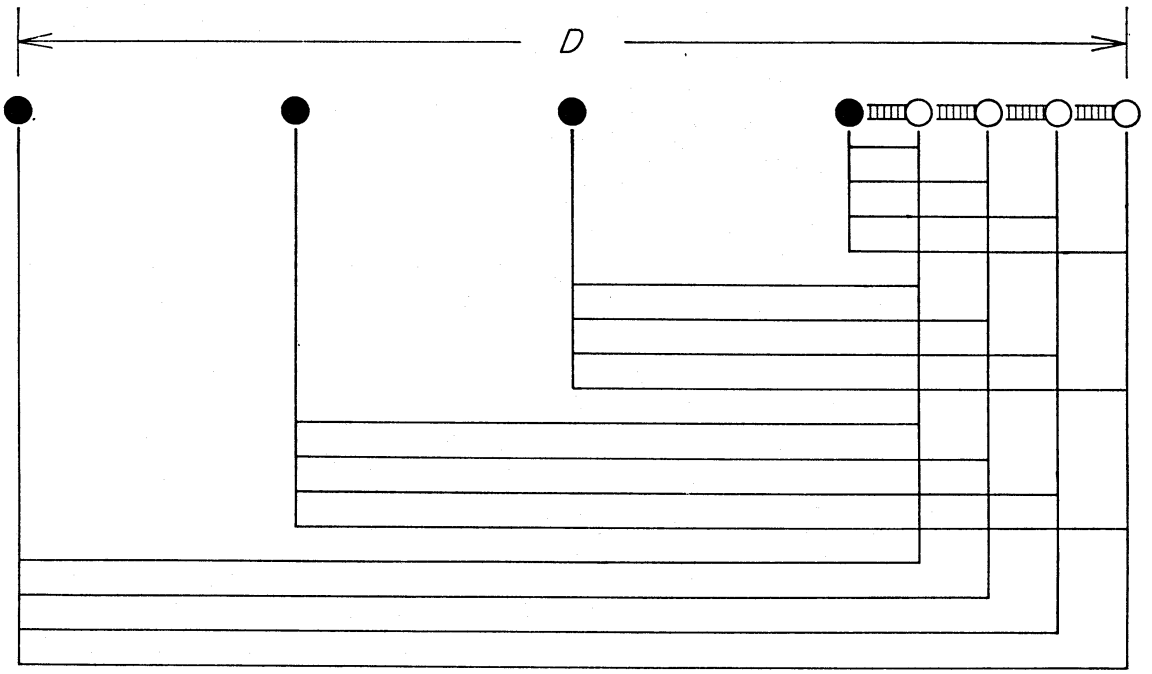

FIG. 2. *The method of combining eight aerials to give* 16 *separations which are in increments of* 1/16 *of the maximum separation D. The black aerials are fixed whilst the white aerials can be moved along tracks towards the nearest black aerial, providing separations which are intermediate between those shown.*

where eight aerial elements are arranged along an east–west axis, providing 16 spacings which are used simultaneously. Four of the eight aerials are movable, and can be arranged along a rail track to fill in further spacings, so that maps comprising 16, 32, 64 or 128 spacings can be obtained in 1, 2, 4 or 8 runs each of 12-hr duration. The effects of irregular refraction on the response pattern of the instrument are determined first, followed by a consideration of the effects of curvature and gradients. Finally the overall limitations imposed by atmospheric refraction are derived. The effects of atmospheric refraction on other designs of telescope will depend on the configuration of the elements, and on the sampling time required for each observation in relation to the characteristic time scale of the phase fluctuations. Whilst it is impossible to give any general expression, the relationships derived for the present design may be applied to other designs.

6.1 *The effects of atmospheric irregularities*

Once the physical characteristics of the atmosphere are known, the performance of a given design of radio telescope can be ascertained in the following way:

(i) Series of path errors along lines of sight to each element are generated from random numbers according to methods described in detail by Hinder (1971). The series are correlated from element to element according to the spatial scale of the irregularities, and their time scale is related both to the scale size and to the velocity with which the irregularities cross the instrument.

(ii) For each spacing of the elements used in the synthesis (shown in Fig. 2) series of differential path errors are derived. Phase departures are subsequently obtained, of magnitude proportional to λ for tropospheric irregularities, and λ^{-1} for ionospheric irregularities.

(iii) Phase departures calculated for a simulated observation of 12-hr duration are then imposed on the phases computed for a point source, and a map of the point source is made by performing a two-dimensional Fourier transformation.

(iv) The loss of gain resulting from the phase variations is found by comparison with a map obtained in the absence of phase departures.

(v) A map of the sidelobes alone is generated by subtracting from each spacing the contribution to the main response and repeating the Fourier transformation. This map enables a more precise analysis of the magnitude and distribution of the sidelobe responses to be made. The level of sidelobes is expressed as a fraction α of the *reduced* main response which can then be compared directly with the maximum tolerable levels derived in Section 3.

The simulated phase departures derived in this way should be statistically indistinguishable from the phase departures which would arise in a real observation; the resulting behaviour of the sidelobe level with λ and D is accordingly well determined from our present knowledge of the characteristics of atmospheric irregularities.

A wide variety of both tropospheric and ionospheric irregularities was simulated to determine their effects on a range of telescopes having baselines from 100 to 1000 km and operating at wavelengths from 0·1 cm to 10 m. The tropospheric irregularities were chosen to have scale sizes from 300 to 1200 m, moving in directions parallel, perpendicular, and at 45° to the baseline, at speeds from 3 to 10 m s^{-1}.

An example of the phase departures obtained for a telescope of total extent 10 km using the procedure presented by Hinder (1971) is shown in Fig. 3; the tropospheric irregularities have a scale size of 700 m, and move with a velocity of 5 m s^{-1} across the telescope at 45° to the baseline. The vertical scale is arbitrary, and is the same for each spacing. The magnitude of the phase departures varies only slightly with spacing, since the scale size is about the same as the smallest aerial spacing shown. The effects of correlation can be seen between the different series.

In the case of the ionospheric irregularities scales of 100 and 200 km were assumed with speeds from 100 to 300 m s^{-1}, giving characteristic times between about 6 min and 33 min.

An example of phase departures which simulate the effects of ionospheric irregularities is presented in Fig. 4. The irregularities have a scale size of 100 km and move across the telescope with a velocity of 100 m s^{-1}. The maximum baseline is again 10 km, and the phase departures are shown for the same spacings as in

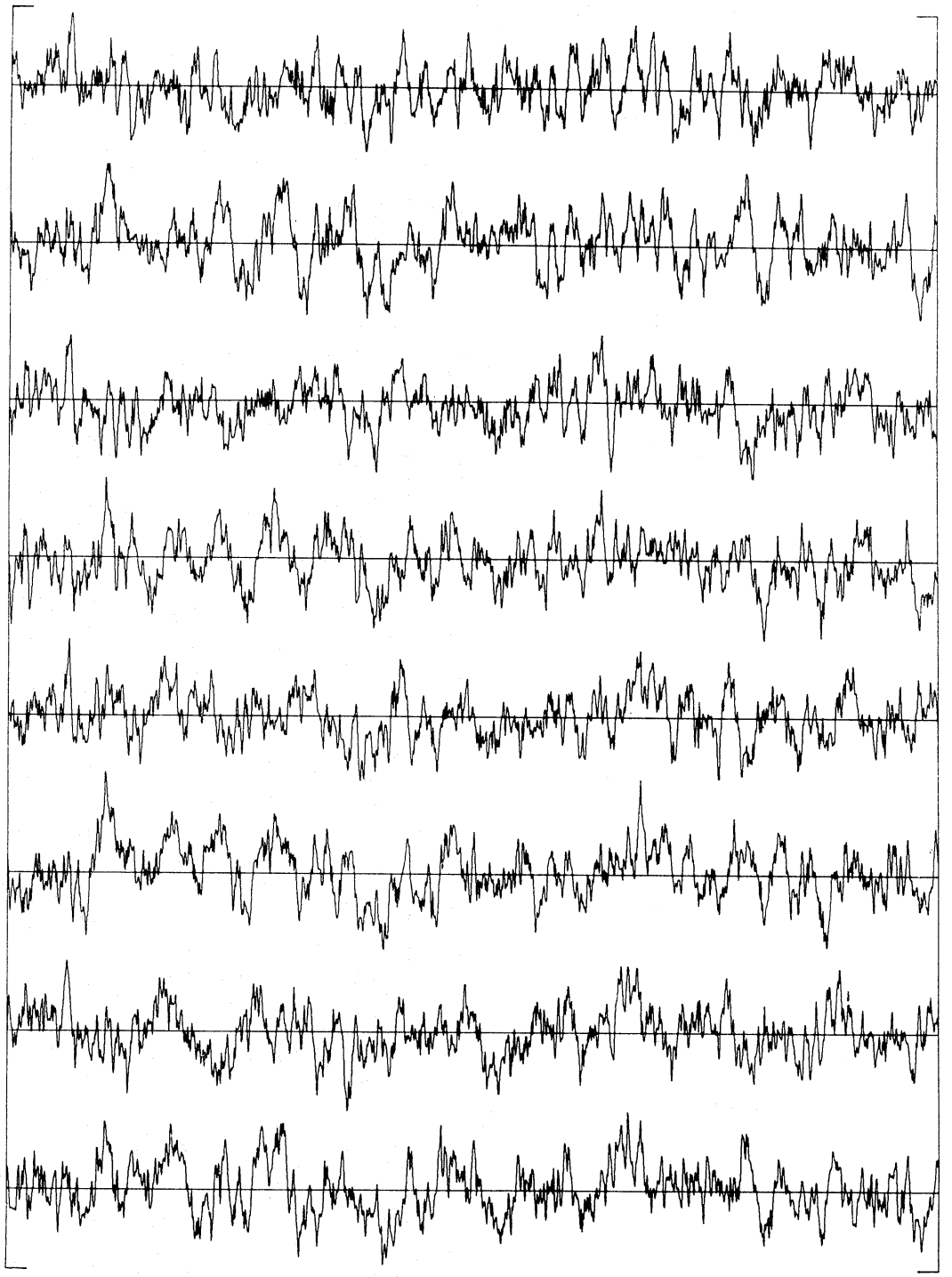

FIG. 3. *Simulated phase departures typical of tropospheric irregularities passing over a telescope of the design shown in Fig. 2. The baselines increase from top to bottom and for clarity only the 2nd, 4th, 6th, etc. spacings are shown; the total duration of the records is 6 hr.*

Fig. 3. The vertical scale is the same for each spacing but otherwise arbitrary. Owing to the large scale size of the irregularities relative to the extent of the telescope, the magnitude of the phase departures is approximately proportional to the separation of the aerials and the different series are highly correlated.

In all, over 100 simulated sets of observations were analysed.

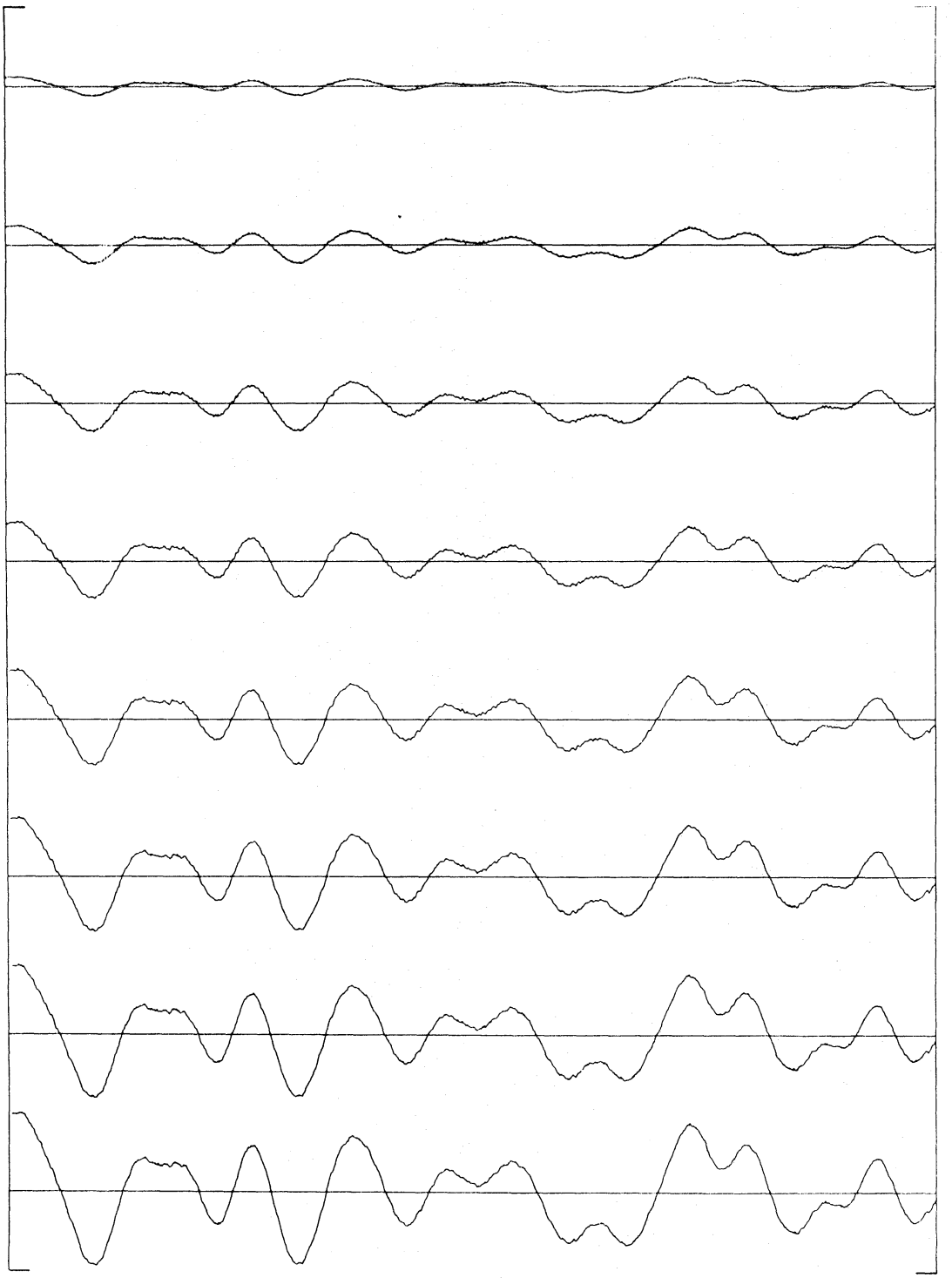

FIG. 4. *Simulated phase departures typical of ionospheric irregularities passing over a telescope of the design shown in Fig. 2. The baselines increase from top to bottom and for clarity only the 2nd, 4th, 6th, etc. spacings are shown, for a total duration of 6 hr.*

Two examples of the sidelobe maps derived using this procedure are shown in Figs 5 and 6, where the maximum baseline D is 10 km; each map is the result of observations made simultaneously on 16 spacings for a total duration of 12 hr. Fig. 5 is an example of the sidelobes produced at $\lambda \approx 1$ cm by irregularities in the troposphere typical of those occurring in the summer day-time. The structure of

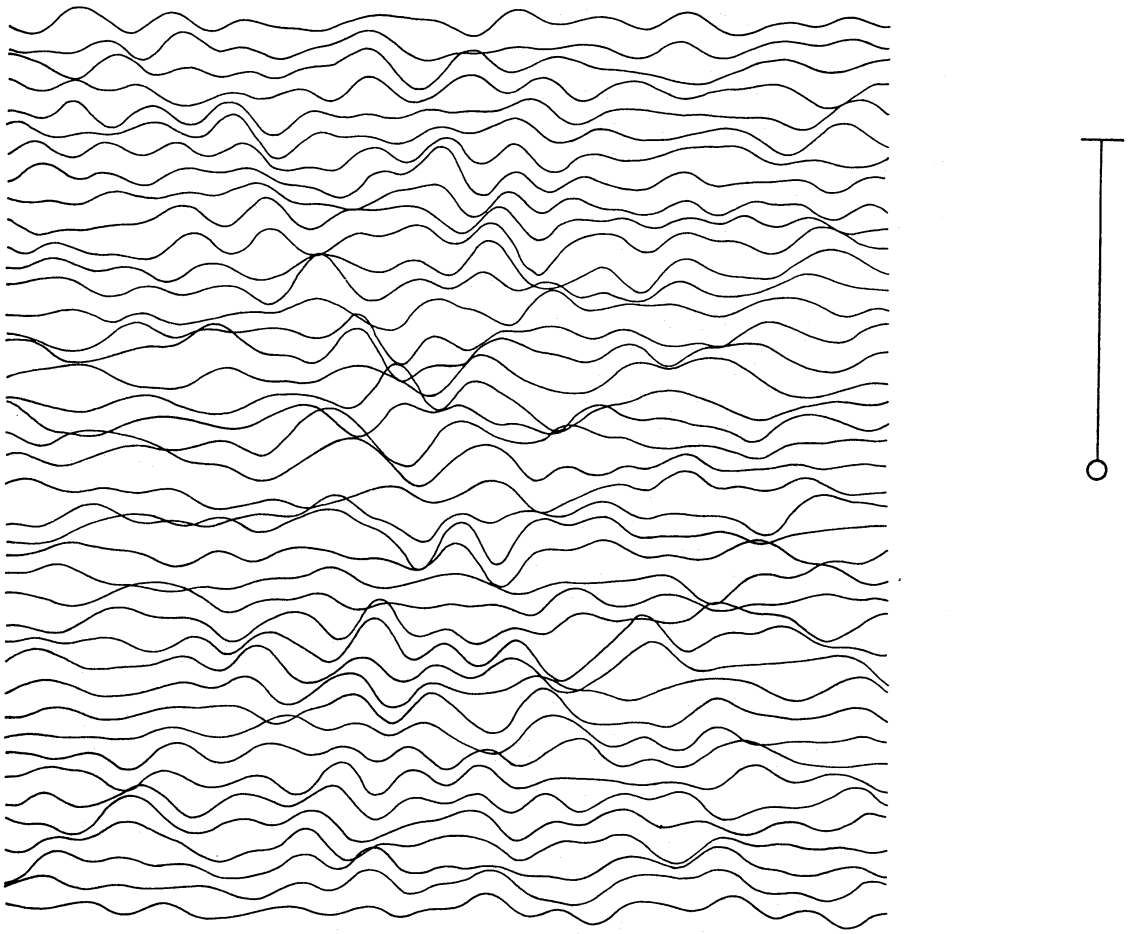

FIG. 5. *Sidelobes characteristic of phase variations imposed at* $\lambda = 1$ *cm by irregularities of refractive index in the troposphere during the summer day-time on an instrument having* 16 *spacings and a maximum baseline of* 10 *km. The height of the main response is indicated on the right together with a circle of radius equal to the r.m.s. sidelobe level over a circular area whose boundary extends up to the edges of the map. The sidelobe level is smaller at longer wavelengths.*

the sidelobes is almost random, but in places the effects of the correlation arising from the simultaneous observation of the 16 spacings can be seen as radial ridges. Fig. 6 is an example of the effects produced at $\lambda \approx 2$ m by ionospheric irregularities having a r.m.s. variation of path length along the line of sight of $1{\cdot}0\,\lambda^2$ m, which is a little larger than the average value. The correlation effects are more marked than in Fig. 5 owing to the larger scale of the ionospheric irregularities which, in this case, is much greater than the maximum baseline of the instrument and therefore introduces a correlation over all spacings as well as over several consecutive samples observed on each spacing. In both Figs 5 and 6 the edges of the map are half-way to the first grating responses, which are circular about the main response. In both cases the sidelobe levels are some 3 per cent r.m.s. relative to the main response.

Each of the sidelobe maps can be characterized by the r.m.s. sidelobe level occurring over the whole map, since the sidelobe level varies only slightly with angular distance from the main response. Fig. 7 illustrates this point with an analysis of maps into rings concentric with the main response; the results have been derived from four simulations for each of the tropospheric and ionospheric irregularities characteristic of Figs 5 and 6. In both cases the r.m.s. sidelobe level over the whole

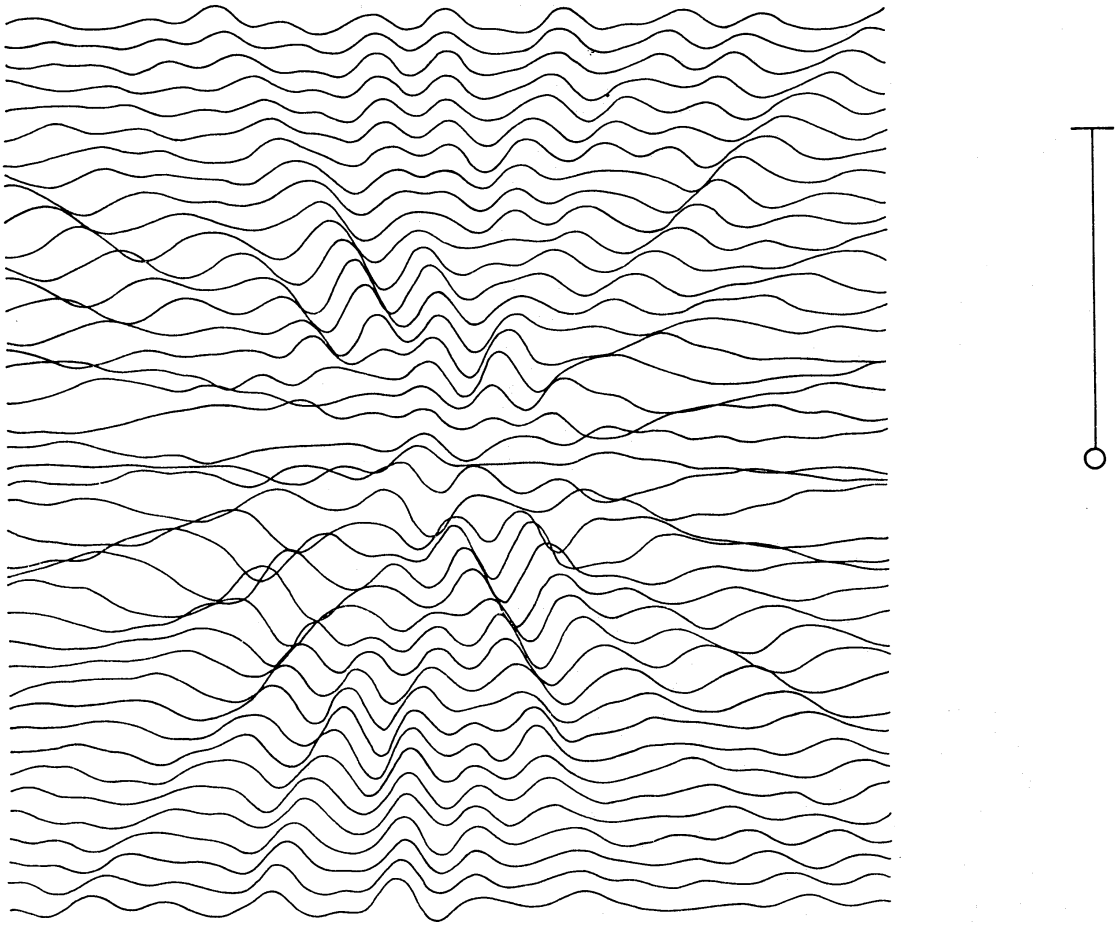

FIG. 6. *Sidelobes characteristic of phase variations imposed at* $\lambda = 2$ *m by irregularities of refractive index in the ionosphere on an instrument having* 16 *spacings and a maximum baseline of* 10 *km. The height of the main response is indicated on the right, together with a circle of radius equal to the r.m.s. sidelobe level over a circular area whose boundary extends up to the edges of the map. The sidelobe level is smaller at shorter wavelengths.*

area of the primary response is about 3 per cent. There is a tendency for the sidelobe variations to increase nearer the main response, particularly for the ionospheric case, but over the whole of the primary response shown in Fig. 7 the variation about the mean value is sufficiently small to render the mean r.m.s. sidelobe level a useful parameter for characterizing the complete map. The variation of the sidelobe level with angular distance from the main response is generally of the form shown in Fig. 7, although the details naturally depend on the assumed characteristics of the irregularities. It should be noted that the examples displayed in Figs 5, 6 and 7 refer to sidelobes imposed on the response of an instrument having a maximum baseline of 10 km by tropospheric irregularities at $\lambda \approx 1$ cm (Fig. 5) and by ionospheric irregularities at $\lambda \approx 2$ m (Fig. 6). The level of sidelobes imposed by the ionospheric irregularities decreases as the wavelength of observation decreases, whilst that imposed by the tropospheric irregularities decreases as the wavelength of observation increases. This behaviour will now be described in more detail in terms of the phase variations imposed by the irregularities, and may be compared with the simplified analysis of Section 2.

As the line of sight phase variations increase, the sidelobe level increases relative to the main response, and the latter decreases relative to that obtained in the absence

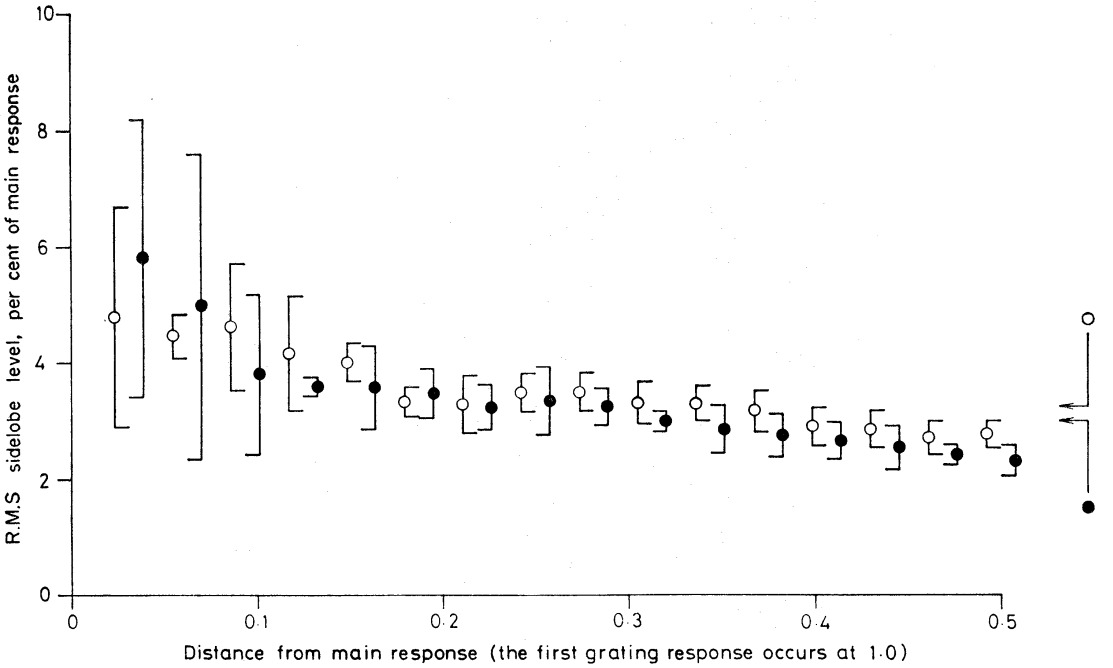

FIG. 7. *Examples of the variation of sidelobe level with angular distance from the main response. The results are characteristic of the sidelobes shown in Figs* 5 *and* 6. *The open circles represent the behaviour for tropospheric irregularities, the closed circles that for ionospheric irregularities. The error bars are standard deviations, calculated from four simulated observations, each having the same characteristics apart from different random numbers. The r.m.s. sidelobe levels over the whole of the primary response of the grating synthesis (which extends half-way to the first grating response) are indicated on the right. It should be noted that the sidelobe levels are a marked function of the observing wavelength.*

of phase variations. The precise relationship between the sidelobe level, or the main response, and the r.m.s. phase variation is again dependent on the statistical characteristics of the phase variations and the number of spacings used. The overall behaviour is, however, exemplified by that shown in Fig. 8 for tropospheric irregularities having the same characteristics as those used in the simulation of Fig. 5. The lines *A* and *B* refer to maps obtained with 16 and 128 spacings respectively. It is seen that, for the smaller values of phase variation (which in the case of tropospheric irregularities would occur at the longer wavelengths), the sidelobe level, shown as a fraction of the *reduced* main response, is proportional to the r.m.s. phase variation as was indicated by the simplified analysis of Section 2; for larger values of phase variation, the sidelobe level increases more and more rapidly until the main response is no longer distinguishable. The dashed vertical line indicates the maximum r.m.s. line of sight phase variation which, for these particular irregularities and an instrument having 16 spacings on a maximum baseline of 10 km, will produce sidelobes of less than 1 per cent r.m.s. which, according to the criteria adopted in Section 3, is acceptable to the mapping of fairly complex sources. For sources of larger angular extent it may be necessary to observe on more than 16 spacings by moving the four movable aerials to intermediate positions along the rail track. A map comprising observations from 128 spacings is then simply the sum of eight component maps each having sidelobes characteristic of a 16 spacing synthesis, since the range of baselines does not, on the whole, alter much as the aerials are moved. Since the eight successive observations must be

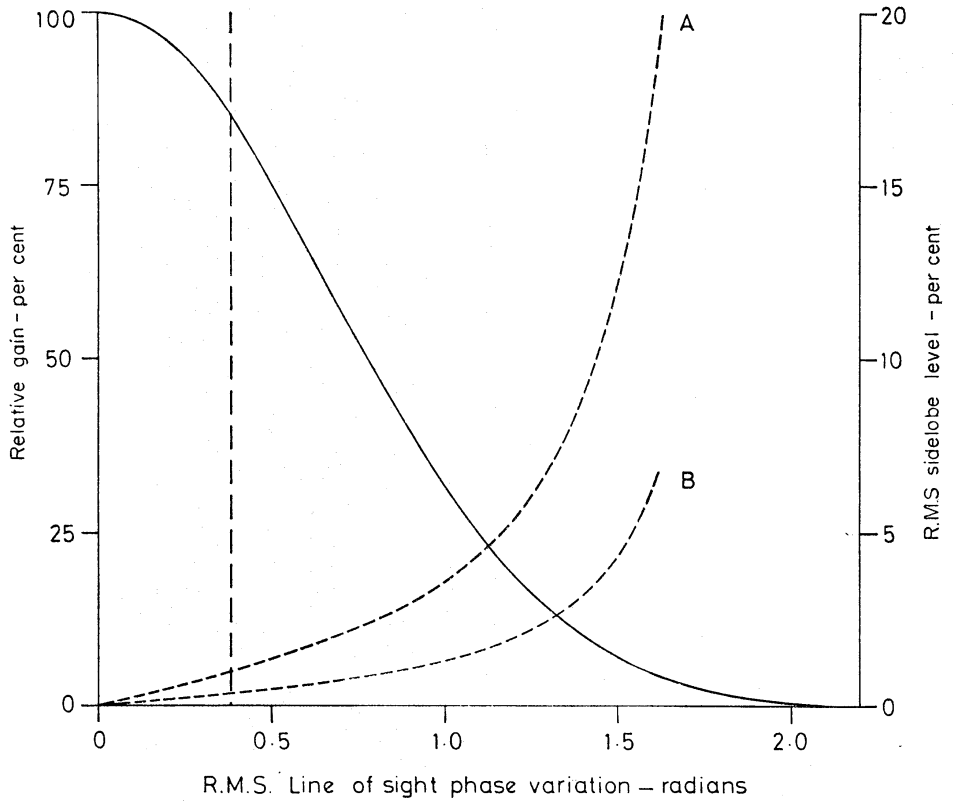

FIG. 8. *The behaviour of the main response (full line) and sidelobe levels (dashed lines) with increasing line of sight phase variation, for tropospheric irregularities having a scale size of 700 m moving at an angle of 45° relative to the baseline of a 10 km telescope at 5 m s^{-1}. Curves* A *and* B *apply to syntheses of 16 and 128 spacings (comprising 8 separate runs of 16 spacings) respectively. The vertical dashed line indicates the maximum r.m.s. line of sight phase variation which is tolerable in observations of complex sources.*

made on different occasions the sidelobes are statistically independent, although having a similar r.m.s. level. Consequently the level of 1 per cent which applies to a single observation of 12-hr duration reduces to a level of $\approx 0{\cdot}3$ per cent for a synthesis of 128 spacings, a factor of $8^{1/2}$ better as shown by B in Fig. 8.

The loss of forward gain of the instrument depends simply on the magnitude of the phase departures whilst the sidelobe responses are also dependent on their time scale. In all practical cases the sensitivity is degraded significantly by phase variations greater than the value which produces a sidelobe level of a few per cent r.m.s.

Results obtained from the full range of simulated observations are presented as a graph (Fig. 9) of isopleths of constant r.m.s. sidelobe level as a function of the operating wavelength λ and the maximum baseline D; the isopleths represent regions where, in temperate latitudes, sidelobes of better than the indicated values will be achieved for 50 per cent of the time. The increase of the sidelobe level at the shorter wavelengths is imposed by tropospheric irregularities. For baselines larger than 10 km the curves are shown dashed since they have been derived from experiments which would not have revealed scale sizes much greater than ~ 10 km. At longer wavelengths the sidelobe level increases due to the presence of ionospheric irregularities.

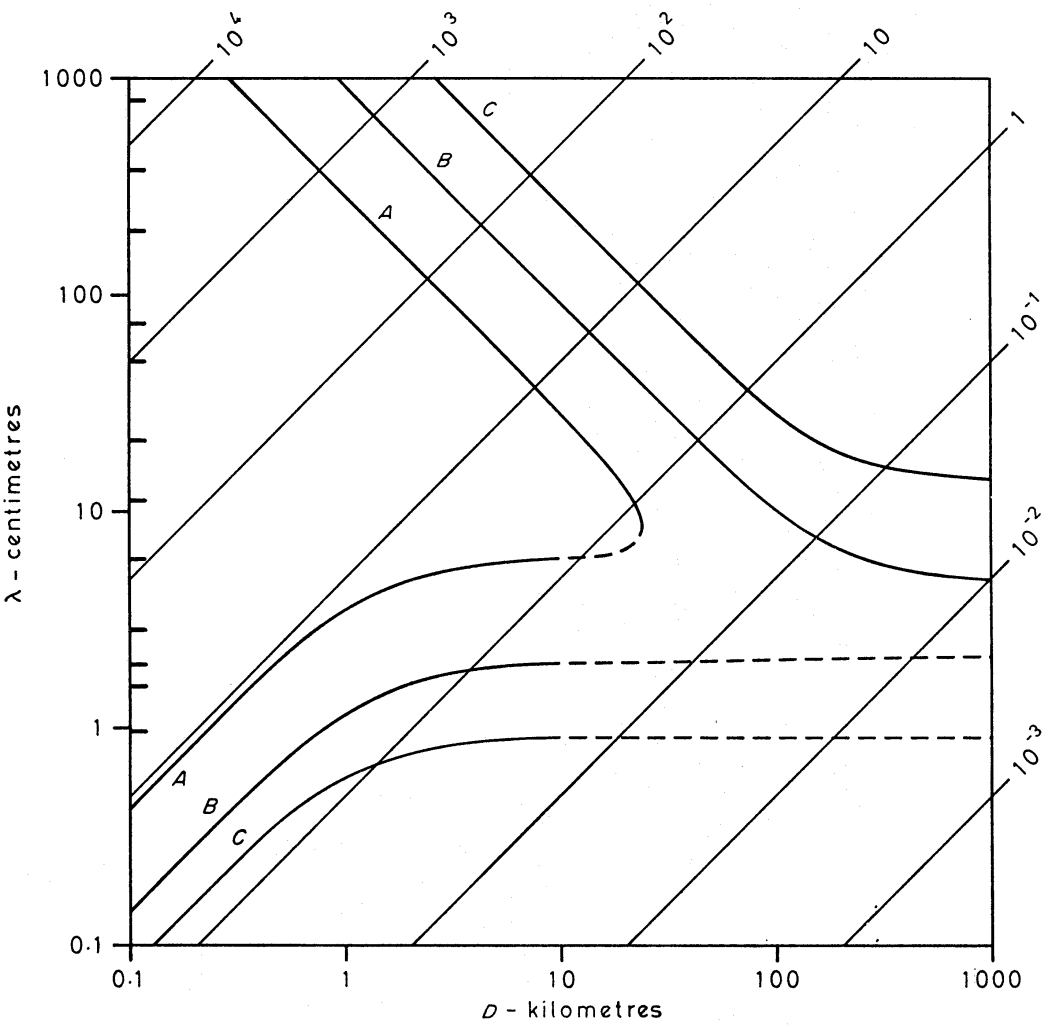

FIG. 9. *Isopleths of r.m.s. sidelobe level plotted as a function of the observing wavelength* λ *and the maximum aerial separation D. Curves* A, B *and* C *refer to sidelobe levels of* 0·3, 1 *and* 3 *per cent r.m.s. for a* 16 *spacing synthesis, and to* 0·1, 0·3 *and* 1 *per cent (approximately) for a synthesis of* 128 *spacings. A sidelobe level of better than the indicated values will be achieved for* 50 *per cent of the time for observations in temperate latitudes. The diagonals are lines of constant angular resolution, marked in seconds of arc. The radio astronomy bands are indicated on the right of the wavelength axis.*

Lines of constant resolution (λD^{-1}) are also shown in Fig. 9, and it can be seen that, in the absence of large scale atmospheric effects, a resolution of 1″ arc should be possible for instruments having a maximum baseline of ~10 km, operating at wavelengths in the region of 6 cm; at larger baselines and slightly shorter wavelengths a resolution of 0·1″ arc may be possible for some of the time.

6.2 *The effects of gradients and curvature*

It is now pertinent to examine what further restrictions on λ and D are imposed by the gradients and curvature of the atmosphere. It can be seen from Tables II and V that the differential paths due to gradients are generally less important than those arising from the curvature of the atmosphere, whilst the effects which they produce—notably sidelobes close to the main response—are similar. Consequently an analysis of the effects of curvature alone is sufficient to cover the effects of both curvature and gradients.

The path difference imposed by curvature results from the different elevation angles of a source observed simultaneously by two aerials. It is zero for a source normal to the baseline, i.e. on the meridian of an east–west baseline, but is finite elsewhere, increasing rapidly at small angles of elevation (as shown in Tables II and V) particularly in the case of the troposphere. For baselines up to ~1000 km the differential path change imposed by the curvature of both the troposphere and the ionosphere is proportional to the baseline. The instantaneous effect is therefore to alter the apparent position of the source under observation. In equatorial co-ordinates the source appears to move during a run of 12-hr duration in an arc having a centroid which is shifted in declination but not in right ascension from the true position of the source. The overall effect of curvature is therefore to introduce an apparent change of declination and to generate sidelobes close to the main response. The apparent declination is lower than the true declination in the

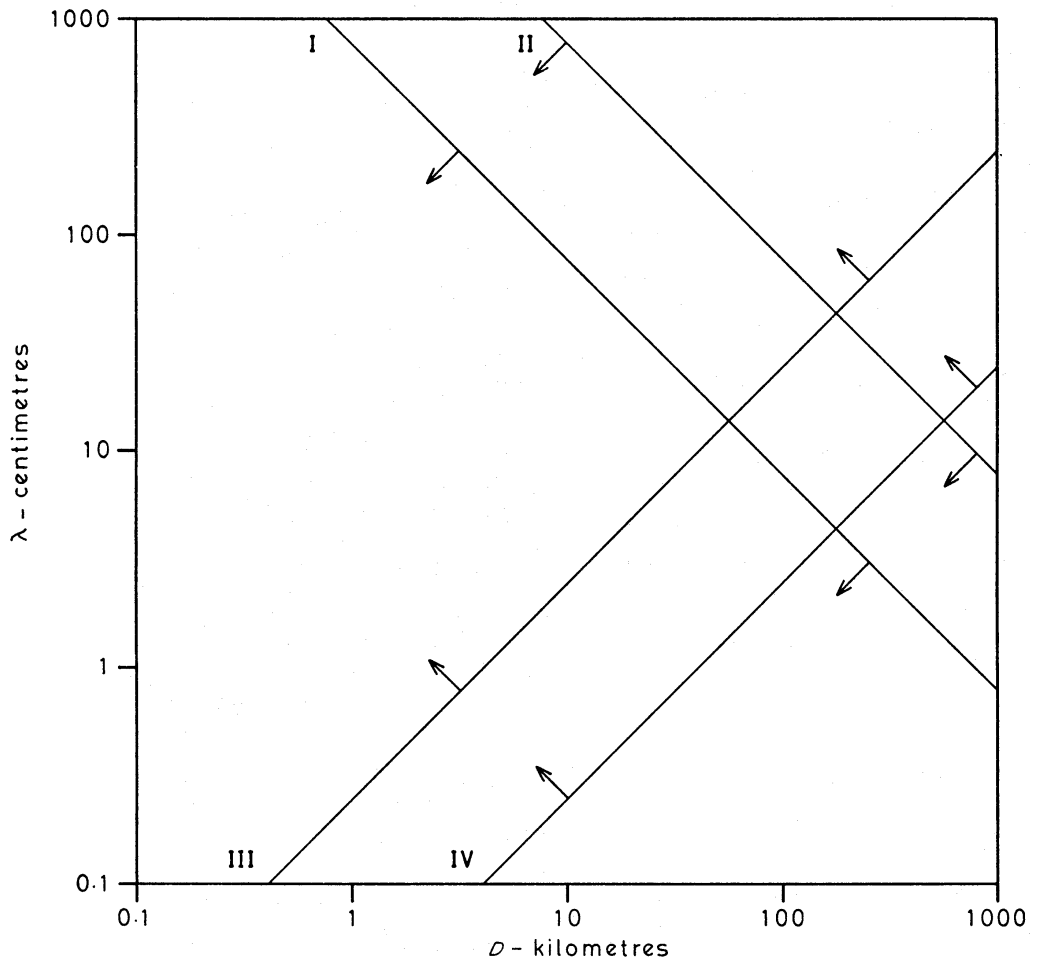

FIG. 10. *Limits imposed by the curvature of the atmosphere on the observing wavelength λ and the maximum baseline D. The permissible regions of operation lie on the sides of the lines indicated by the arrows. The limits apply to an instrument located in middle latitudes observing sources at declination 20°. For observations at higher declinations the limits are less severe than those shown here. Lines I and III are the limits imposed by the curvature of the ionosphere (corrected with an accuracy of 10^{17} electrons m^{-2}) and the troposphere (corrected with an accuracy of 10 per cent) respectively. Lines II and IV are the probable limits to which observations might be extended, given the accuracy of currently proposed methods of correction.*

case of tropospheric refraction, and higher for ionospheric refraction. It was suggested in Sections 4 and 5 that the path changes due to curvature could be estimated to within 10 or 20 per cent by straightforward measurements. It is assumed in the following discussion that such corrections are made, and that the limitations are due to the residual effects.

The major limitation in the mapping of sources is likely to arise from the near-in sidelobes, and it is assumed that their maximum tolerable limit is 10 per cent r.m.s. of the main response. This figure corresponds to a r.m.s. phase error about the value corresponding to the shift of declination which is $\approx 0{\cdot}2$ rad on the maximum baseline. For a source at a given declination, observed from a given latitude, the r.m.s. phase change due to curvature can be derived to a sufficient accuracy from the concentric slab models of the troposphere and ionosphere used in the calculation of Tables II and V. Fig. 10 shows the limiting wavelengths derived from this procedure for an instrument in middle latitudes and for a source at declination 20°. The limits are less severe for sources at higher declinations. The lines drawn in Fig. 10 consequently show the regions where the effects of curvature must be seriously considered, and are not to be interpreted as rigorous boundaries. The line I in Fig. 10 assumes that straightforward estimates of the total electron content, from e.g. ionosonde measurements, to within 10^{17} electrons m^{-2} of the true value, are available and that appropriate corrections are made. The line II is the probable limit to which the observations could be extended if the residual uncertainty in the total electron content of the ionosphere were 10^{16} electrons m^{-2} throughout the period of observation. Such an accuracy might be achieved in observations of Faraday rotation of satellite signals. The effect of the troposphere should be predictable to within 10 per cent from measurements of surface pressure, temperature and humidity; the line III indicates the residual limitation. It is possible that measurements of atmospheric parameters along the lines of sight throughout the troposphere would enable the effect to be corrected with a residual error of 1 per cent, in which case the line IV would apply. The limits I and III therefore represent the limits of λ and D which are imposed on an instrument in middle latitudes by the systematic refraction of the atmosphere when straightforward measurements are used to correct the effect. With the aid of extensive and more sophisticated measurements the limits might be extended to the lines II and IV.

6.3 *The overall effect of atmospheric refraction*

The previous results can now be combined with a knowledge of the probability distribution of the line of sight path changes ΔL to derive, for a given instrument, the overall limitations imposed by atmospheric refraction. The variability of the irregular ionospheric path changes is indicated in Table III, and the variability of the tropospheric component is known from observations by Hinder (1970, and further work in preparation).

For an instrument having a maximum baseline of 10 km, and observing simultaneously on 16 spacings in middle latitudes, the proportion of time for which a sidelobe level of better than 1 per cent relative to the main response will be achieved is shown in Fig. 11 as a function of the wavelength of observation. The corresponding figure for a synthesis of 128 spacings, comprising eight sets of observations of 16 spacings each, according to the scheme of Fig. 2, is 0·3 per cent. The wave-

lengths at which the effects of curvature produce 10 per cent sidelobes close to the main response are indicated by dashed lines; they correspond to the residual limitations discussed previously and shown in Fig. 10.

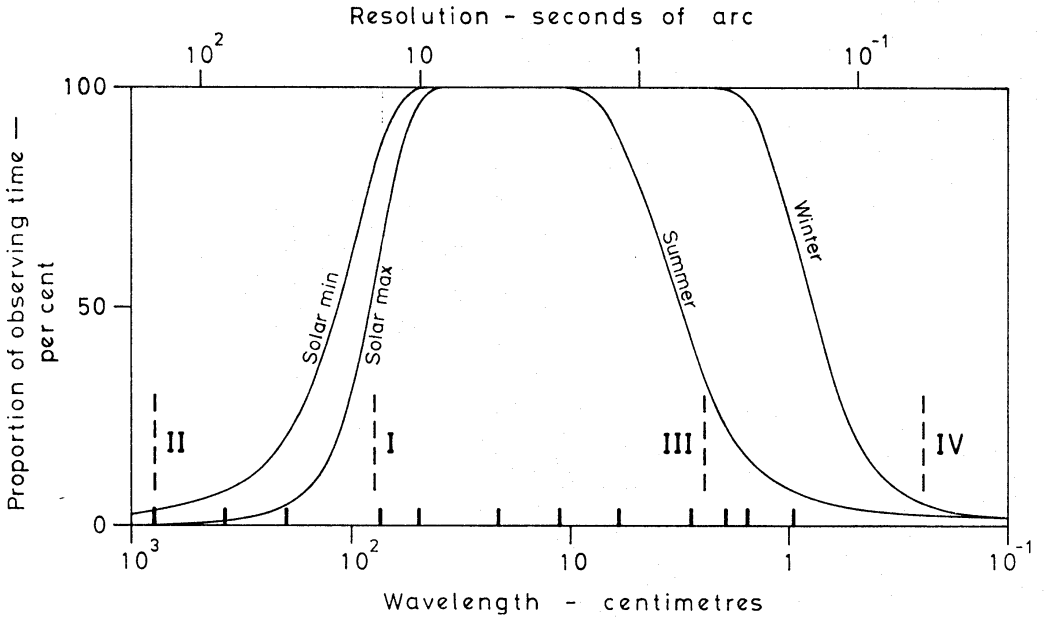

FIG. 11. *The proportion of time for which a sidelobe level of better than 1 per cent will be achieved in syntheses of 16 spacings using an instrument having a maximum baseline of 10 km in temperate latitudes. The dashed vertical lines I–IV correspond to the limits imposed by the curvature of the atmosphere, shown in Fig. 10. The bands allocated to radio astronomy are indicated along the wavelength axis.*

At longer wavelengths the restrictions are due to ionospheric refraction; the limitations due to irregularities are shown separately for sunspot maximum and minimum. At shorter wavelengths the observing time is limited by tropospheric refraction; curves for the irregular component are shown separately for summer and winter. Each curve includes the variability due to different scale sizes and velocities in addition to the inherent variability of ΔL. The winter curve is not well known since it is based on few data, many of which are upper limits. Whilst observations might be feasible at wavelengths shorter than those indicated by the winter curve it should be noted that at wavelengths less than about 2 cm additional problems arise from the absorption of radio waves by water vapour, oxygen, clouds and precipitation.

In order to scale Fig. 11 to other baselines, the wavelengths of the appropriate limits should be scaled according to the isopleths of Figs 9 and 10.

Whilst these results are strictly applicable only to conditions prevailing in middle latitudes, an indication of conditions at other locations can be derived as follows. The tropospheric irregularities are almost certainly associated with changes in water vapour content arising from convective activity (Hinder in preparation). They are correlated with the presence of cumulus cloud and, from data on such cloud in the U.S. (Cunningham 1962), it appears that at lower latitudes the variations may, throughout the year, be up to three times larger than the summer value found in middle latitudes. At latitudes greater than Cambridge (52° N) the insolation is lower and there is less water vapour in the air; the varia-

tions are therefore expected to be smaller. It follows that at latitudes nearer the equator the wavelength restrictions imposed by the tropospheric irregularities may be a factor of three larger than those shown in Fig. 11 for the summer curve and are then appropriate to day-time observations throughout the year. At night-time the shorter wavelength limit is likely to fall between the curves shown in Fig. 11 for summer and winter. At latitudes greater than about 70°, on the other hand, the shorter wavelength limit may be near that of the winter curve at all times. There are insufficient data on the ionospheric irregularities to permit a geographical analysis, but from data on the total electron content (Garriott *et al.* 1970) it appears that the limitations imposed by the curvature of the ionosphere are least restrictive in middle latitudes.

7. CONCLUSIONS

Experience gained in the operation of the One-Mile telescope at 5 GHz has shown that it should be technologically feasible to build much larger synthesis instruments than are at present under construction. The resolving power which can be obtained on the surface of the Earth is, however, limited by refraction occurring in the atmosphere. Ionospheric irregularities having a scale size of about 100 km preclude the successful operation of large synthesis telescopes at the longer wavelengths, whilst tropospheric irregularities having a scale size of about 1 km became a hindrance at the shorter wavelengths. The permissible observing wavelengths and baselines are further limited by the systematic refraction due to the curvature of the atmosphere. In principle the effects of both the irregular and systematic refraction occurring in the atmosphere are amenable to correction but would require the development of techniques which are likely to be difficult to apply in practice, particularly if attempting to correct for the effects of irregular refraction. It appears that the range of operating wavelengths which would enable complex sources to be reliably mapped would, for an instrument having a maximum baseline of 10 km, be restricted to the range ≈ 2 cm to ≈ 100 cm, provided that the observations were corrected to first order for refraction arising from the curvature of the atmosphere and did not extend to elevations less than 15°. The angular resolution achieved by such an instrument would be in the range $\approx 0{\cdot}4$ to ≈ 20 sec of arc.

Instruments of larger physical size would be limited to a smaller range of operating wavelengths, and maps at greater resolution could only be obtained if extensive measurements were made to correct for the effects of atmospheric curvature.

The evaluation of an observing site for high resolution radio astronomy requires a knowledge both of the irregularities and of the total refraction occurring in the atmosphere over the site. For the ionosphere, this might be obtained either from measurements of the Faraday rotation or changes of the phase path length of a beacon signal from a geostationary satellite, or from the angular deviation of sources observed with a radio interferometer. For the troposphere, path changes might be investigated either by ground-based measurements of the altitude profiles of temperature and humidity, using microwave radiometry (Schaper *et al.* 1970) or laser back-scattering (Cooney 1970), or by interferometric observations of point radio sources.

ACKNOWLEDGMENTS

We thank Dr J. R. Shakeshaft and Dr J. E. Baldwin for comments on the manuscript, and Dr S. Kenderdine and Peter Warner for help with the computing. During the course of this work Richard Hinder was supported by the Science Research Council, the Cavendish Laboratory and Corpus Christi College, Cambridge.

Mullard Radio Astronomy Observatory, Cavendish Laboratory, Cambridge.

Received in original form 1971 *March* 22

REFERENCES

Almeida, O. G., Garriott, O. K. & da Rosa, A. V., 1970. *Planet. Space Sci.*, **18,** 159.
Baars, J. W. M., 1967. *IEEE Trans. Ant. Propag.*, **AP-15,** 582.
Basart, J. P., Miley, G. K. & Clark, B. G., 1970. *IEEE Trans. Ant. Propag.*, **AP-18,** 375.
Bean, B. R. & Dutton, E. J., 1966. *Radio Meteorology*, Natn. Bur. Stand. Monogr., No. 92.
Bhonsle, R. V., 1966. *J. geophys. Res.*, **71,** 4571.
Clarke, M. E., 1964. Ph.D. Thesis, University of Cambridge.
Cooney, J., 1970. *J. appl. Met.*, **9,** 182.
Cooney, J., Orr, J. & Tomasetti, C., 1969. *Nature*, **224,** 1098.
Cunningham, R. M., 1962. *Geophys. Res. Pap.*, **No. 51.**
Davies, K., 1965. *Ionospheric Radio Propagation*, Natn. Bur. Stand. Monogr., No. 80.
Dickinson, D. F., Grossi, M. D. & Pearlman, M. R., 1970. *J. geophys. Res.*, **75,** 1619.
Elsmore, B., Kenderdine, S. & Ryle, M., 1966. *Mon. Not. R. astr. Soc.*, **134,** 87.
Garriott, O. K., da Rosa, A. V. & Ross, W. J., 1970. *J. atmos. terr. Phys.*, **32,** 705.
Garriott, O. K. & Smith, F. L., 1965. *Planet. Space Sci.*, **13,** 839.
Gent, H., Adgie, R. L. & Crowther, J. H., 1969. *RRE Newsl. Res. Rev.*, **No. 8, paper 25.**
Hewish, A. & Symonds, M. D., 1969. *Planet. Space Sci.*, **17,** 313.
Hinder, R. A., 1970. *Nature*, **225,** 614.
Hinder, R. A., 1971. Ph.D. Thesis, University of Cambridge.
Lawrence, R. S., Jesperson, J. L. & Lamb, R. C., 1961. *Bur. Stand. J. Res.*, **65D,** 333.
Mathur, N. C., Grossi, M. D. & Pearlman, M. R., 1970. *Radio Sci.*, **5,** 1253.
Murray, C. A., Tucker, R. H. & Clements, E. D., 1969. *Nature*, **221,** 1229.
Okoye, S. E. & Hewish, A., 1968. *J. atmos. terr. Phys.*, **30,** 163.
Rao, N. N., 1967. *J. geophys. Res.*, **72,** 2929.
Rickett, B. J., 1970. *Mon. Not. R. astr. Soc.*, **150,** 67.
Roger, R. S., 1964. *J. atmos. terr. Phys.*, **26,** 499.
Ryle, M. & Hewish, A., 1960. *Mon. Not. R. astr. Soc.*, **120,** 220.
Schaper, L. W., Staelin, D. H. & Waters, J. W., 1970. *Proc. Inst. electr. electron. Eng.*, **58,** 272.
Titheridge, J. E., 1968. *J. atmos. terr. Phys.*, **30,** 73.
Williams, P. J. S., 1964. Ph.D. Thesis, University of Cambridge.